Theoretical Study on the f−f Transition Intensities of Lanthanide Trihalide Systems†

Miho Hatanaka and Satoshi Yabushita*

School of Fundamental Science and Technology, Graduate School of Keio University, 3-14-1 Hiyoshi, Kohoku-ku, Yokohama 223-8522, Japan

Received: May 27, 2009; Revised Manuscript Received: August 3, 2009

The photoabsorption intensities of intra-$4f^N$ transitions (f−f transitions) in lanthanide systems have been extensively studied with the semiempirical Judd−Ofelt theory. The oscillator strengths of most f−f transitions are insensitive to a change of surrounding environment because 4f electrons are shielded by closed-shell 5s and 5p electrons from outside. However, there are some exceptional transitions, so-called hypersensitive transitions, whose intensities are very sensitive to a change of surrounding environment, and the reason for this hypersensitivity has not been clarified. In this study, we calculated the oscillator strengths of lanthanide trihalides (LnX_3; Ln = Pr, Tm; X = Br, I) with the multireference spin−orbit configuration interaction method and obtained reasonably accurate values. To clarify the cause of hypersensitivity, we examined various possible effects on the oscillator strengths, such as molecular vibration, f−d mixing, ligand to metal charge transfer (LMCT), and intraligand excitation, and concluded that the effect of molecular vibration is very small and that the oscillator strengths of most f−f transitions including hypersensitive transitions arise from both the LMCT and dynamic-coupled intraligand excitations through their configuration mixings with the dominant configurations of $4f^N$.

1. Introduction

Intra-$4f^N$ electronic transitions (f−f transitions) in lanthanide systems are of interest due to the usefulness for optical materials, and nonempirical calculations of their oscillator strengths are an important challenge. The oscillator strengths of f−f transitions have long been investigated with semiempirical theory called the Judd−Ofelt theory.[1,2] Although f−f transitions are Laporte forbidden, in the Judd−Ofelt theory, their finite intensities have been interpreted to arise because opposite parity states $|c\rangle$, such as $4f^{N-1}5d^1$, are mixed into $4f^N$ states due to the presence of odd parity crystal or ligand fields V_{odd}, and $4f^N$ states are perturbed as

$$|\Psi_{4f^N}\rangle = |(4f^N)_a\rangle + \sum_c |c\rangle \frac{\langle c|V_{odd}|(4f^N)_a\rangle}{E_a - E_c} \quad (1)$$

According to the Judd−Ofelt theory, the oscillator strengths of f−f transitions induced by odd parity force fields are written as

$$f_{FI} = \frac{2\chi}{3(2J+1)}\omega_{FI}\sum_{t=2,4,6}\Omega_t|\langle\Psi_F(S',L',J')||U^{(t)}||\Psi_I(S,L,J)\rangle|^2 \quad (2)$$

where Ω_t values ($t = 2, 4, 6$) are Judd−Ofelt parameters, which depend on the strengths and the properties of force fields; $U^{(t)}$ are reduced tensor operators; χ is the Lorentz field correction; Ψ_I and Ψ_F are the initial and final state wave functions, respectively; and ω_{FI} is the excitation energy from Ψ_I to Ψ_F. If these wave functions are expressed in the Russell−Saunders coupling scheme, the matrix elements of $U^{(t)}$ can readily be evaluated. Because eq 2 is expressed by only three Ω_t parameters, which are independent of the excited levels, the oscillator strengths of all kinds of transitions can be obtained by those of only three transitions measured by absorption or emission spectrum of the system. Oscillator strengths of many lanthanide systems have been successfully explained by the Judd−Ofelt theory. According to the recent review,[3] this theory has been used in about 800 investigations to report intensities of lanthanide systems.

4f electrons are affected little by the surrounding environment because they are well shielded by closed-shell 5s and 5p electrons from outside. Therefore, the crystal or ligand field splittings are smaller than the spin−orbit (SO) splittings, and the electronic states of the lanthanide trivalent ion (Ln^{3+}) in crystal or ligand fields are usually similar to those of free Ln^{3+}. Although the electronic states are labeled by the Russell−Saunders scheme ($^{2S+1}L_J$), only the total angular momentum J is assumed to remain a good quantum number because of the large SO effect.

In spite of the shielding effect, there are some exceptional f−f transitions whose oscillator strengths are very sensitive to a small change of surrounding environment. These transitions have been called "hypersensitive transitions" by Jørgensen and Judd[4] and have been extensively studied.[3,5] The hypersensitive transitions obey the selection rules as $|\Delta J| \leq 2$, $|\Delta L| \leq 2$, and $\Delta S = 0$, and their oscillator strengths are usually enhanced greatly compared with those of Ln^{3+} in aqueous solution. Especially, Gruen et al.[6,7] observed that the oscillator strengths of hypersensitive transitions in gaseous lanthanide trihalide (LnX_3) molecules were much larger than those of Ln^{3+} in solutions or crystals.

Several reasons for this hypersensitivity have been propounded. Judd noticed that the matrix elements of $U^{(2)}$ in eq 2 were large for hypersensitive transitions and that the Ω_2 parameters were sensitive to a small change of surrounding environment. In general, the Judd−Ofelt theory can give good

† Part of the "Russell M. Pitzer Festschrift".

* To whom correspondence should be addressed. E-mail: yabusita@chem.keio.ac.jp. Fax: +81-45-566-1697.

10.1021/jp9049507 CCC: $40.75
Published on Web 09/11/2009

agreement between experimental and calculated oscillator strengths, because Ω_2 parameters were treated as empirical parameters and adjusted to experimental values. This theory has not been employed to give a nonempirical explanation for the hypersensitivities. Later, Judd included the crystal-field parameters in the expression for Ω_2 and argued that the hypersensitivities occurred in certain limited point groups, such as C_s, C_1, C_2, C_3, C_4, C_6, C_{2v}, C_{3v}, C_{4v}, and C_{6v}.[8] This theory could be confirmed by several experimental results.[8,9] However, there are exceptions to the theory. The most significant one is the gaseous LnX_3 molecules[7] mentioned above. They have D_{3h} symmetry and notably large oscillator strengths for hypersensitive transitions. Therefore, it cannot be the whole explanation, although this theory can explain some aspects of hypersensitivity.

To explain the great enhancement of the oscillator strengths of hypersensitive transitions in gaseous LnX_3 systems, Gruen et al.[7] examined a number of mechanisms and explained that the hypersensitivity was attributable to the molecular vibration. The symmetries of these molecules can be lowered effectively because the frequencies of their out-of-plane bending vibrations are very small and the oscillator strengths were measured under the high temperature condition at about 1000 K. Henrie et al.[10] explained their large oscillator strengths by means of a vibronic mechanism with the inclusion of covalency between lanthanide and ligands. However, the vibronic mechanism was criticized by many authors.[5]

The covalency model mentioned above is one of the proposed models to explain the hypersensitivity. If the charge-transfer character is included in f−f intensities, the hypersensitivity to the surrounding ligands is understandable because the energies and intensities of the charge-transfer transitions are very sensitive to the kind of ligands and metals. Henrie et al.[11] modified the Judd−Ofelt theory by including charge-transfer states in addition to the opposite parity states $4f^{N-1}5d^1$. However, this mechanism was also criticized.[5,12]

The dynamic-coupling (DC) model, which considered the ligand-polarization contributions to the oscillator strengths, was advocated by Mason, Peacock,[13−15] and others.[16−19] In this model, it is interpreted that the intensities of pseudoquadrupolar hypersensitive f−f transitions in Ln^{3+} complexes arise principally from the Coulombic correlation between the transition quadrupole moment of the metal ion and induced electric dipoles in the ligands. It is noted that, in the Judd−Ofelt theory, ligands are treated as point charges, and the perturbing wave functions are localized exclusively on the central lanthanide ion. The DC model can explain the great enhancement of Ω_2 in gaseous LnX_3.

These large numbers of old studies have been carried out based on experiments or semiempirical theories, and the calculations of oscillator strengths of their f−f transitions have not been carried out with the ab initio method, although those in actinide systems have been studied by Pitzer et al.[20] In this study, the oscillator strengths of LnX_3 are calculated by the multireference spin−orbit configuration interaction (SOCI) method, and the cause of f−f transitions and hypersensitivity in particular is examined. We compare several calculation methods in section 4.1, calculate the oscillator strengths of LnX_3 in section 4.2, and examine the cause of the f−f transitions and the hypersensitivity in sections 4.3 through 4.5. Especially, we focus on the following points: molecular vibration, f−d mixing, ligand to metal charge transfer excitations, and intraligand excitations.

2. Theory

2.1. Two Formulas of Transition Dipole Moment. As is well-known, the transition dipole moment which gives optical transition probability between two quantum states is expressed in length form (LF) and velocity form (VF). If the wave functions are the eigenfunctions of the Schrödinger equation, LF is derived using the eigenvalue expressions as

$$\langle \Psi_F | [H^{\mathrm{SF}}, \sum_{j=1}^{N} \mathbf{r}_j] | \Psi_I \rangle = (E_F - E_I) \langle \Psi_F | \sum_{j=1}^{N} \mathbf{r}_j | \Psi_I \rangle \quad (3)$$

where H^{SF} is the spin-free Hamiltonian; E_I and E_F are the eigenvalues of Ψ_I and Ψ_F, respectively, that are the eigenfunctions of H^{SF}; and N is the number of electrons. VF is derived from the direct commutation operation of H^{SF} and the coordinate operator as

$$\langle \Psi_F | [H^{\mathrm{SF}}, \sum_{j=1}^{N} \mathbf{r}_j] | \Psi_I \rangle = \langle \Psi_F | - \sum_{j=1}^{N} \frac{\partial}{\partial \mathbf{r}_j} | \Psi_I \rangle \quad (4)$$

These two forms give an equal value if they are calculated with the exact eigenfunctions.

For systems containing heavy atoms with significant SO effects, the Hamiltonian needs to include the SO interaction term. In this case, the LF operator does not change the form since

$$\langle \Psi_F^{\mathrm{SO}} | [H^{\mathrm{SF}} + H^{\mathrm{SO}}, \sum_{j=1}^{N} \mathbf{r}_j] | \Psi_I^{\mathrm{SO}} \rangle = (E_F^{\mathrm{SO}} - E_I^{\mathrm{SO}}) \langle \Psi_F^{\mathrm{SO}} | \sum_{j=1}^{N} \mathbf{r}_j | \Psi_I^{\mathrm{SO}} \rangle \quad (5)$$

where H^{SO} is the SO Hamiltonian; and $E_I^{\mathrm{SO}}$and E_F^{SO} are the eigenvalues of Ψ_I^{SO} and Ψ_F^{SO}, respectively, that are the eigenfunctions of $H^{\mathrm{SF}} + H^{\mathrm{SO}}$. On the other hand, VF needs to include the correction term,[21] which is represented as a commutator of H^{SO} and the coordinate operator as in

$$\langle \Psi_F^{\mathrm{SO}} | [H^{\mathrm{SF}} + H^{\mathrm{SO}}, \sum_{j=1}^{N} \mathbf{r}_j] | \Psi_I^{\mathrm{SO}} \rangle = \langle \Psi_F^{\mathrm{SO}} | - \sum_{j=1}^{N} \frac{\partial}{\partial \mathbf{r}_j} + [H^{\mathrm{SO}}, \sum_{j=1}^{N} \mathbf{r}_j] | \Psi_I^{\mathrm{SO}} \rangle \quad (6)$$

In this study, we use two forms of H^{SO}. One is an approximate one-body SO Hamiltonian[22] as

$$H^{\mathrm{SO}} \approx \frac{\alpha^2}{2} \sum_{j}^{N} \sum_{A}^{\mathrm{atom}} \frac{Z_{\mathrm{eff}}(A)}{r_{jA}^3} \mathbf{l}_{jA} \cdot \mathbf{s}_j \quad (7)$$

where α is the fine structure constant and $Z_{\mathrm{eff}}(A)$ is an effective nuclear charge of the Ath atom determined to reproduce the experimental SO splitting. When SO Hamiltonian is expressed as in eq 7, the correction term for VF can be written as

$$[H^{\mathrm{SO}}, \sum_{j=1}^{N} \mathbf{r}_j] = i \frac{\alpha^2}{2} \sum_{j=1}^{N} \sum_{A=1}^{\mathrm{atom}} \frac{Z_{\mathrm{eff}}(A)}{r_{jA}^3} \{\mathbf{r}_{jA} \times \mathbf{s}_j\} \quad (8)$$

The other H^{SO} form is expressed as a one-electron SO operator[23−25] as

$$H^{SO} = \sum_{j=1}^{N} \mathbf{s}_j \cdot \sum_{A=1}^{\text{atom}} \sum_{l_A=1}^{L_A} \xi_{l_A}(r_{jA}) \mathbf{O}_{l_A} \mathbf{l}_{jA} \mathbf{O}_{l_A} \tag{9}$$

where $\mathbf{O}_{l_A}$ is the projection operator defined as

$$\mathbf{O}_{l_A} = \sum_{m=-l_A}^{l_A} |l_A m\rangle\langle l_A m| \tag{10}$$

and the radial function in eq 9 is usually derived from relativistic effective potentials, as follows

$$\xi_{l_A}(r_{jA}) = \frac{2}{2l_A + 1} \Delta U_{l_A}^{\text{REP}}(r_{jA}) \tag{11}$$

When the SO Hamiltonian is expressed as in eq 9, the correction term for VF has a one-electron operator form

$$[H^{SO}, \sum_{j=1}^{N} \mathbf{r}_j] = \sum_{j=1}^{N} \sum_{A=1}^{\text{atom}} \sum_{l_A=1}^{L_A} [\mathbf{O}_{l_A} \xi_{l_A}(r_{jA}) \{\mathbf{l}_{jA} \cdot \mathbf{s}_j\} \mathbf{O}_{l_A}, \mathbf{r}_j] \tag{12}$$

A program to compute matrix elements of these correction terms in eqs 8 and 12 over Gaussian atomic basis was coded and attached to the COLUMBUS program system.[26] In what follows, transition moments are given only in LF for simplicity; however, those in VF are also calculated to assess the reliability of theoretical calculations.

2.2. Effect of Molecular Vibration on Oscillator Strength. If vibrational degrees of freedom are taken into consideration, photoabsorption intensity at a photon frequency ω consists of many vibronic transitions, each of which is proportional to the squares of transition dipole moments between initial and final vibronic states, described as follows

$$\sum_{v',v''} \langle \chi_{v'}^F | \mathbf{M}_{FI} | \chi_{v''}^I \rangle \cdot \langle \chi_{v''}^I | \mathbf{M}_{IF} | \chi_{v'}^F \rangle W_{v''} \delta(E_{v'}^F - E_{v''}^I - \omega) \tag{13}$$

where $\chi_{v''}^I$ and $\chi_{v'}^F$ are vibrational wave functions on the electronic states I and F, respectively. $E_{v''}^I$ and $E_{v'}^F$ are their vibronic energies with symbolic vibrational quantum numbers v'' and v'; and $\mathbf{M}_{FI}$ is the geometry-dependent electronic transition dipole moment. $W_{v''}$ is the Boltzmann distribution factor of the initial electronic state.

As is well-known, 4f-electrons have a negligibly small contribution to chemical bonds, and relevant potential energy surfaces for the electronic states I and F in f−f transitions are very similar in shape. Their vertical energy difference is almost independent of molecular geometry. This characteristic allows us to use the common normal coordinates $\mathbf{Q}$ for the electronic states I and F and to assume no photoabsorption intensity unless $v'' \approx v'$. With these considerations, eq 13 can be simplified to the following expressions

$$\begin{aligned}
&\delta(E_F - E_I - \omega) \sum_{v',v''} \langle \chi_{v'}^F | \mathbf{M}_{FI} | \chi_{v''}^I \rangle \cdot \langle \chi_{v''}^I | \mathbf{M}_{IF} | \chi_{v'}^F \rangle W_{v''} \\
&= \delta(E_F - E_I - \omega) \sum_{v',v''} \int \chi_{v'}^F(\mathbf{Q})^* \mathbf{M}_{FI}(\mathbf{Q}) \chi_{v''}^I(\mathbf{Q}) \mathrm{d}\mathbf{Q} \cdot \\
&\qquad \int \chi_{v''}^I(\mathbf{Q}')^* \mathbf{M}_{IF}(\mathbf{Q}') \chi_{v'}^F(\mathbf{Q}') \mathrm{d}\mathbf{Q}' \cdot W_{v''} \\
&= \delta(E_F - E_I - \omega) \sum_{v''} \iint \mathrm{d}\mathbf{Q}\mathrm{d}\mathbf{Q}' \delta(\mathbf{Q} - \mathbf{Q}') \mathbf{M}_{FI}(\mathbf{Q}) \chi_{v''}^I(\mathbf{Q}) \cdot \\
&\qquad \chi_{v''}^I(\mathbf{Q}')^* \mathbf{M}_{IF}(\mathbf{Q}') \cdot W_{v''} \\
&= \delta(E_F - E_I - \omega) \int \mathrm{d}\mathbf{Q} \mathbf{M}_{FI}(\mathbf{Q}) \cdot \mathbf{M}_{IF}(\mathbf{Q}) \sum_{v''} \chi_{v''}^I(\mathbf{Q})^* \chi_{v''}^I(\mathbf{Q}) \cdot W_{v''}
\end{aligned} \tag{14}$$

where the contributions to all the vibrational states $\chi_{v'}^F(\mathbf{Q})$ on the final electronic state F are summed over, and the completeness relation has been used. To estimate the impact of each normal vibration i on the oscillator strength, we evaluate the above integrals only along normal coordinate Q_i, with keeping $Q_j = 0$ ($j \neq i$), that is

$$f_i^{FI} = \int \mathrm{d}Q_i f'^{FI}_i(Q_i) \sum_{v''} |\chi_{v''}^I(Q_i)|^2 W_{v''} \tag{15}$$

where $f'^{FI}_i(Q_i)$ is the oscillator strength function calculated at normal coordinate Q_i. This integral f_i^{FI} can be interpreted as an averaged oscillator strength calculated with the weight of the existing probability function.[27]

3. Calculation Methods

3.1. Praseodymium Trivalent Ion. From the discussion in the Introduction, theoretical methods in this study are required to yield accurate transition moments for 4f to 5d excited states. To assess this requirement, ab initio calculations were performed for free ion Pr^{3+} by the SOCI method using the COLUMBUS program package.[26,28] We compared five calculation methods that are the relativistic effective core potential (RECP) method by Cundari et al.[29] denoted as RECP(A), the small-core RECP method by Dolg et al.[30] with the SO operator denoted as RECP(B), that with the approximate one-body SO Hamiltonian in eq 7 denoted as RECP(C), the model core potential (MCP) method,[31,32] and the all-electron nonrelativistic Hartree−Fock (HF) method. The valence shells of RECP(A) and MCP methods are 4f5s5p5d6s, and those of RECP(B) and RECP(C) methods are 4s4p4d4f5s5p5d6s. We employed a primitive (6s,6p,3d,7f) GTO basis set[29] for RECP(A), (12s,11p,9d,8f)/[9s,8p,6d,5f] basis set[30] and a spherical d-polarization function ($\alpha_d = 0.16$) for RECP(B) and RECP(C), (10s,7p,7d,6f)/[5s,3p,4d,4f] basis set[31,32] for the MCP, and (19s,16p,11d,8f)/[13s,10p,7d,5f] basis set[33] and a spherical d-polarization function ($\alpha_d = 0.16$) for the all-electron HF method. The approximate one-body SO Hamiltonians in eq 7 were used except for RECP(B), and the value of Z_{eff} was determined to reproduce the experimental SO splittings[34] of low-lying $4f^2$ excited states of the trivalent ion. Note that the same parameter Z_{eff} was used for other atomic orbitals as well. We employed the state-averaged SCF molecular orbitals (MOs) that were optimized for the averaged state of all the configurations derived from $(4f5d)^2$. For the SOCI calculations, singlet and triplet configuration state functions (CSFs) were generated with the reference of $(4f5d)^2$ in the first-order and second-order CI. The first-order CI calculation included all the CSFs in the reference plus a full set of CSFs generated by distributing one hole in the internal (doubly occupied and active)

space and one electron in the external space in all possible ways. The second-order SOCI calculation further included up to two holes in the internal space and up to two electrons in the external space in all possible ways.

3.2. Lanthanide Trihalides. Ab initio calculations were performed for LnX_3 (Ln = Pr, Tm; X = Br, I) by the SOCI method using the COLUMBUS program package. The geometries of LnX_3 were D_{3h} with the experimental bond lengths[35] 5.08, 5.48, 4.88, and 5.27 (Bohr) for $PrBr_3$, PrI_3, $TmBr_3$, and TmI_3, respectively. We used the MCPs by Sakai et al. The valence shells of MCP-DZPs[32,36] are 3d4s4p for Br and 4d5s5p for I. We used (8s,7p,8d)/[3s,3p,3d] basis sets[32,36] for halogens. Z_{eff} values for halogens were determined to reproduce the experimental SO splittings[37] between $^2P_{3/2}$ and $^2P_{1/2}$ of the neutral atoms.

To determine the appropriate one-electron orbitals and the CI scheme for LnX_3, in section 4.1, we will compare three calculation schemes for $PrBr_3$: (a) the state-averaged SCF MOs optimized for the averaged state of all the configurations derived from $4f^2$ and singlet and triplet CSFs generated with the reference of $4f^2$, (b) the same state-averaged SCF MOs as in (a) and singlet and triplet CSFs generated with the reference of $(4f5d)^2$, and (c) the state-averaged SCF MOs optimized for the averaged state of all the configurations derived from $(4f5d)^2$ and singlet and triplet CSFs generated as in (b). In these calculations, the CSFs are generated in the first-order CI scheme.

In sections 4.2 through 4.5, we will employ the state-averaged SCF MOs that are optimized for the averaged state of all the configurations derived from $4f^N$ of Ln. For the SOCI calculations, singlet and triplet CSFs are generated in the first-order CI scheme with the reference of $4f^N$ of Ln. In these calculations, a rather large doubly occupied space consisting of $5s^25p^6$ of Ln and $(ns^2np^6)_3$ of X_3 ($n = 4$ for Br and $n = 5$ for I) and also large external space consisting of all the SCF virtual orbitals are used, so that all the relevant one-electron excitations for Ln f−d mixing, LMCT, and intraligand excitations could be simultaneously accounted for.

All the electronic states of LnX_3 correlated with $^{2S+1}L_J$ of Ln^{3+} are also named $^{2S+1}L_J$. The oscillator strengths from initial states $^{2S+1}L_J$ to final states $^{2S'+1}L'_{J'}$ were therefore expressed as

$$f(^{2S'+1}L'_{J'} \leftarrow {}^{2S+1}L_J) = \frac{2}{3(2J+1)} \sum_{k=1}^{2J'+1} \sum_{l=1}^{2J+1} (E_k - E_l)\langle k|\sum_{j=1}^{N} \mathbf{r}_j|l\rangle^2 \tag{16}$$

where l and k are all the states included in $^{2S+1}L_J$ and $^{2S'+1}L'_{J'}$, respectively, and E_l and E_k are their electronic energies. In the second-quantized form, the transition dipole moment from a state Ψ_I to a state Ψ_F can be written as

$$\begin{aligned} \mathbf{M}_{FI} &= \langle\Psi_F|\sum_{j=1}^{N} \mathbf{r}_j|\Psi_I\rangle \\ &= \sum_{f,i} \langle\phi_f|\mathbf{r}|\phi_i\rangle\langle\Psi_F|\sum_{\sigma} a^+_{f\sigma}a_{i\sigma}|\Psi_I\rangle \\ &= \sum_{f,i} \langle\phi_f|\mathbf{r}|\phi_i\rangle\rho^{FI}(f,i) \end{aligned} \tag{17}$$

where ϕ is the molecular orbital; the operators $a^+_{f\sigma}$ and $a_{i\sigma}$ are the fermion creation and annihilation operators for an electron in spatial orbital f and i, respectively, with spin σ; and $\rho^{FI}(f,i)$ is the transition density matrix element. We coded and attached a program to compute the transition density matrix with the graphical unitary group approach (GUGA)[38,39] to the COLUMBUS program package and used it for the calculations of the oscillator strengths.

3.3. Vibrational Wave Function. Full geometry optimization and vibrational analysis of $PrBr_3$ were carried out on the GAMESS[40] program system with the MCPs. The vibrational wave functions in eq 15 were obtained by the finite difference grid method (FDM)[41−43] with a Mathematica program. The temperature value in the Boltzmann distribution factor was 1000 K corresponding to the experimental temperature in the vapor phase.[7] The oscillator strength function $f'^{FI}_i(Q_i)$ along each normal coordinate was calculated with the SOCI method with the same calculation level mentioned in section 3.2. The total number of the points representing each potential function ranges from 10 up to 20. The vibrational states $\chi^I_{i'}$, whose populations were larger than 0.001, were included in eq 15.

3.4. MCP Shift Operator. The atomic Hamiltonian for N_v valence electrons in the MCP method can be written as[31,36]

$$H_{mcp} = \sum_{j=1}^{N_v}\left[-\frac{1}{2}\Delta_j + V_{mcp}(r_j) + \sum_{c=1}^{n_{core}} B_c|\psi_c\rangle\langle\psi_c|\right] + \sum_{i>j}^{N_v} r_{ij}^{-1} \tag{18}$$

where $\{\psi_c\}$, (c = 1s, 2s, ..., n_{core}), denotes core orbital functions. The projection operator $\sum B_c|\psi_c\rangle\langle\psi_c|$ is called energy shift operator because the energy levels of core orbitals are shifted. By including the 5d orbital of Pr to this shift operator, the 5d orbital could be shifted to a higher energy region. (Note that the purpose of this shift is different from that of the original MCP shift operators.) The ψ_{5d} orbitals were expanded in terms of Gaussian-type functions[31] with an augmented d-polarization function ($\alpha_d = 0.45$) to reproduce the shape of the 5d orbitals calculated with the all-electron HF method. The values of B_{5d} were set to 0.1, 0.5, 1.0, and 5.0 au.

4. Results and Discussions

4.1. Dependence on Calculation Methods. The transition dipole moments of free Pr^{3+} between the initial state $^3H_4(4f^2)$ and the final states $^3H_5$ and $^1G_4$ $(4f^15d^1)$ were calculated with the RECP by Cundari, the small-core RECP by Dolg, the MCP method, and the all-electron method. The values of Z_{eff} for these four methods were 24.73, 25.50, 23.71, and 22.36, respectively. The excitation energies and the values of LF, VF, and VF with SO correction term are shown in Table 1. The spin-forbidden transition from $^3H_4$ $(4f^2)$ to $^1G_4$ $(4f^15d^1)$ can arise due to the intensity-borrowing mechanism. Because of the strong SO interaction, the actual initial state has admixture components of $^1G_4$ (2.7%) and $^3F_4$ (0.1%), and similarly the final state contains components of $^3H_4$(6.5%), $^3F_4$ (5.5%), and $^3G_4$ (2.5%). Here, the weight of each LSJ state is given in parentheses. It is interesting to point out that these strong admixtures of singlet and triplet components can give rise to a much larger transition dipole moment than that of the spin-allowed transition from $^3H_4$ $(4f^2)$ to $^3H_5$ $(4f^15d^1)$. Comparing the values of VF and VF including SO correction term, the effect of the SO correction term is very small and independent of the calculation methods for both spin-allowed and spin-forbidden transitions. The ratios of VF and LF calculated with RECP methods are much larger than unity, whereas those with MCP and all-electron methods are nearly equal to unity. While LF gives nearly equal values independent of the calculation methods, VF gives significantly larger values for the RECP methods. The difference between the RECP methods and the other methods lies in the shape of

TABLE 1: Squares of Transition Dipole Moments (Debye^2) and Excitation Energies $\Delta E \times 10^{-3}$ (cm^{-1}) of Pr^{3+}

methods[a]	ΔE	LF	VF	VF + corr.[b]	VF/LF[c]
(i) Spin Allowed Transition from $^3H_4(4f^2)$ to $^3H_5$ $(4f^15d^1)$					
second-order CI					
RECP(A)	58.2	0.19	1.94	1.95	10.02
RECP(B)	64.0	0.23	1.98	1.98	8.47
RECP(C)	64.2	0.22	1.87	1.87	8.50
MCP	76.4	0.22	0.24	0.24	1.12
All-el.	79.7	0.21	0.25	0.25	1.18
first-order CI					
MCP	76.0	0.21	0.25	0.25	1.17
All-el.	79.4	0.21	0.25	0.25	1.22
exptl.[d]	65.2				
(ii) Spin Forbidden Transition from $^3H_4$ $(4f^2)$ to $^1G_4$ $(4f^15d^1)$					
second-order CI					
RECP(A)	56.1	4.14	46.28	46.33	11.17
RECP(B)	59.2	2.38	24.76	24.27	10.42
RECP(C)	60.0	1.21	12.01	12.04	9.89
MCP	72.1	1.54	2.16	2.17	1.41
All-el.	75.2	1.45	1.97	1.97	1.36
first-order CI					
MCP	71.5	1.35	2.00	2.00	1.48
All-el.	74.7	1.35	1.91	1.91	1.41
exptl[d]	61.2				

[a] RECP(A) denotes the RECP method by Cundari; RECP(B) denotes the small-core RECP by Dolg with SO potential; and RECP(C) denotes the small-core RECP by Dolg with an approximate one-body SO Hamiltonian. [b] VF with additional correction term induced by SO interaction. [c] Ratio of LF and VF. [d] Experimental excitation energies are from ref 34.

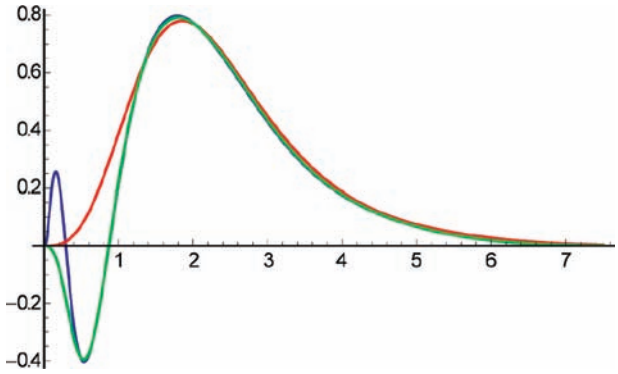

Figure 1. Plot of the radial function ($r\phi$) vs r (in au). Red line is 5d orbital calculated with RECP(A); green line is that with RECP(B); and blue line is that with the all-electron HF method.

their valence orbitals. For example, the radial shapes of the 5d orbital calculated with the RECP methods and the all-electron HF method are shown in Figure 1. The 5d orbital with the MCP method was very similar to that with the all-electron HF method and omitted. The 5d orbital with RECP(A) has nodeless structure, whereas those with MCP and all-electron HF methods have two nodes in the core region. The integrand of LF expressed in the coordinate operator has larger values far from the nucleus and the difference in the core region does not make a significant difference, while that of VF expressed in the derivative operator of the coordinate is sensitive to the nodal structures of orbitals in core regions.[44,45] Therefore, the nodeless feature of the valence orbitals by the RECP(A) can be a reason for the large difference between LF and VF. As seen in Figure 1, the 5d orbital by RECP(B) has a radial node in the core region because 4d electrons are also treated as valence electrons. However, the ratios of VF and LF with the RECP(B) are as large as those with RECP(A); therefore, the addition of one

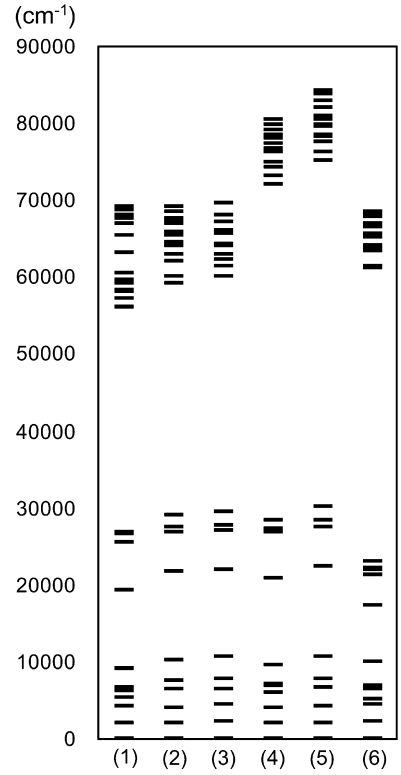

Figure 2. Computed $4f^2$ and $4f^15d^1$ energy level (cm^{-1}) of Pr^{3+} calculated with five methods: (1) RECP(A), (2) RECP(B), (3) RECP(C), (4) MCP, (5) nonrelativistic all-electron, and (6) experimental value.[34] States whose energies are under 30 000 cm^{-1} are $4f^2$ states, and those above 50 000 cm^{-1} are $4f^15d^1$ states.

radial node for the 5d orbital with the small-core RECP does not improve the disagreement between LF and VF. From these results, it is suggested that values of the VF depend critically on the accuracy of wave functions in the core region, especially on the nodal structure of valence orbitals.

We next compared the excitation energies calculated with these methods. As shown in Table 1, the excitation energies of the $4f^15d^1$ states depend on the calculation methods. Especially, those with the MCP or all-electron methods were overestimated compared to the experimental values, whereas those with the RECPs were estimated reasonably. The overestimation of the excitation energies with the all-electron method may be caused by the use of nonrelativistic Hamiltonian. These energies may be improved by using the quasi-relativistic all-electron method. However, as shown in Figure 2, the excitation energies of low-lying $4f^2$ states are fairly similar. Therefore, the MCP method is the most adequate method for this study because the excitation energies and the two forms of transition dipole moments of low-lying $4f^N$ states can be calculated in reasonable accuracy.

Next, the dependence on the expression of the SO interaction term was investigated.[46] We compared RECP(B) and RECP(C) in Table 1. As shown in Table 1, RECP(B) and RECP(C) yield nearly equal values for the excitation energies and the transition dipole moments. Therefore, these two forms of approximate one-body SO Hamiltonians could give reasonably accurate excitation energies and transition dipole moments for states including 5d, even though the Z_{eff} parameter was adjusted to reproduce the experimental SO splittings of low-lying $4f^2$ states.

Next, we compared the first-order and second-order CI schemes. As is shown in Table 1, the differences between these two CI schemes are very small for both excitation energies and transition dipole moments. Moreover the ratios of VF and LF

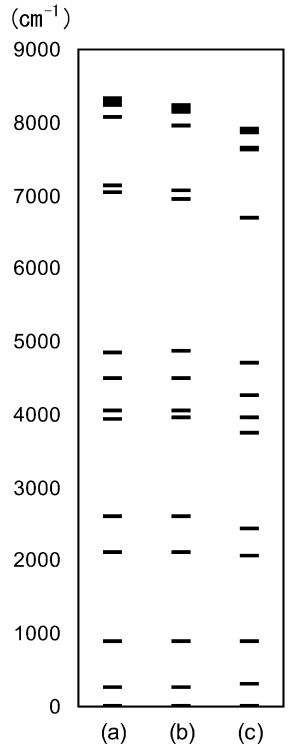

Figure 3. Computed $4f^2$ energy level (cm^{-1}) of $PrBr_3$ with three computational schemes, (a) using MOs averaged in $4f^2$ and treating 4f as active space, (b) using MOs averaged in $4f^2$ and treating 4f and 5d as active space, and (c) using MOs averaged in $(4f5d)^2$ and treating 4f and 5d as active space.

in the first-order CI scheme are similar to those in the second-order CI scheme even though the computational accuracy was reduced. Therefore, it is expected that the relevant properties in this study could be calculated in reasonable accuracy in the first-order CI scheme.

Lastly, the dependence on the active space was investigated for PrX_3. In the calculation of $4f^N$ states in a system without the center of inversion symmetry such as LnX_3, 5d orbitals may need to be included in the active space because opposite parity configurations, such as $4f^{N-1}5d^1$, are variationally mixed into $4f^N$ states, whereas in the case of free Ln^{3+}, opposite parity configurations cannot be mixed in. Therefore, the three SCF and CI calculation schemes explained in section 3.2 were compared. Figure 3 shows the excitation energies of $4f^2$ states of $PrBr_3$ calculated with the three SCF and CI schemes. As is clearly seen, the scheme (c) gave the lowest excitation energies among the three schemes. However, their differences especially for the $4f^2$ states were not large. It is therefore suggested that the properties of $4f^2$ states could be evaluated in reasonable accuracy without including the 5d orbitals in the active space in reference CSFs.

4.2. Oscillator Strengths of Lanthanide Trihalides. On the basis of the results presented in section 4.1, the oscillator strengths of LnX_3 (Ln = Pr, Tm; X = Br, I) were calculated with the MCP method. Table 2 shows the oscillator strengths of PrX_3, and Table 3 shows those of TmX_3. The LF values are in better agreement with experiment than the VF values for both PrX_3 and TmX_3. LF seems to give more reliable values than VF in molecular calculation because of its insensitivity for nodal structure. In section 4.1, we showed that LF gave nearly equal values independent of the calculation methods. Therefore, we tested the calculation of the oscillator strengths of LnX_3 with the RECP(A) method. Compared with the MCP method, the RECP(A) method gave about half the values for the LF oscillator strengths and about a thousand for the ratios of VF and LF.

TABLE 2: Oscillator Strengths ($f \times 10^6$) of PrX_3 from $^3H_4$

states	exptl[a]	LF	VF	VF/LF
		(i) $PrBr_3$		
$^3H_5$	-	1.16	5.13	4.41
$^3H_6$	} 20.0[b]	0.12	0.52	4.34
$^3F_2$		28.08	81.50	2.90
$^3F_3$	} 1.0[c]	3.62	16.12	4.45
$^3F_4$		1.18	3.49	2.96
		(ii) PrI_3		
$^3H_5$	-	2.21	15.26	6.91
$^3H_6$	} 40.0[b]	0.13	2.04	15.25
$^3F_2$		52.91	148.37	2.80
$^3F_3$	} 13.4[c]	7.08	31.14	4.40
$^3F_4$		1.71	4.51	2.64

[a] Experimental oscillator strengths from ref 7. [b] The sum of oscillator strengths to $^3H_6$ and $^3F_2$. [c] The sum of oscillator strengths to $^3F_3$ and $^3F_4$.

TABLE 3: Oscillator Strengths ($f \times 10^6$) of TmX_3 from $^3H_6$

states	exptl[a]	LF	VF	VF/LF
		(i) $TmBr_3$		
$^3F_4$	12.0	7.59	1.71	0.23
$^3H_5$	2.7	2.97	1.10	0.37
$^3H_4$	15.3	12.19	3.59	0.29
$^3F_3$	}3.3[b]	0.56	0.22	0.40
$^3F_2$		0.05	0.06	1.04
$^1G_4$	4.5	4.48	1.42	0.32
		(ii) TmI_3		
$^3F_4$	10.7	10.23	4.69	0.46
$^3H_5$	4.6	4.95	1.11	0.22
$^3H_4$	25.3	22.26	5.53	0.25
$^3F_3$	11.0	0.68	0.70	1.03
$^3F_2$	-	0.09	0.09	1.01
$^1G_4$	-	7.39	1.44	0.19

[a] Experimental oscillator strengths from ref 7. [b] The sum of oscillator strengths to $^3F_3$ and $^3F_2$.

The hypersensitive transitions reported in experimental studies[7] are as follows: from $^3H_4$ to $^3F_2$ for Pr^{3+}, from $^3H_6$ to $^3F_4$ and to $^3H_4$ for Tm^{3+}. As shown in Tables 2 and 3, the oscillator strengths of these hypersensitive transitions are evaluated quantitatively. Note that the molecular symmetry of D_{3h} is not a point group to which the selection rule by Judd[8] is applicable as was mentioned in the Introduction. The irreducible representations of the initial and final states, which carry the largest transition moments, were both E′, and the components of these transition dipole moments were in the direction of the molecular plane ($x,y \in E'$). This result corresponds to the interpretation of the DC model that suggested the components of induced dipole of the halide ligands are the direction of the molecular plane.[13]

4.3. Effect of Molecular Vibration. Full geometry optimization and vibrational analysis of $PrBr_3$ were carried out, and the equilibrium structure and six normal coordinates Q_i's were obtained as shown in Figure 4. The optimized bond lengths of Pr−Br and the symmetry were 5.20 (Bohr) and D_{3h}, respectively, in good agreement with previously obtained results by Cundari et al.[47] This bond length is also in reasonable agreement with a recent theoretical one, 5.15 (Bohr) with CASPT2,[48] and with the experimental one,[35] 5.08 (Bohr). The frequency of each normal vibration, as shown in Table 4, is also in reasonable agreement with the experimental one.[49]

The molecular symmetry is lowered by the normal vibrations except for the totally symmetric stretching vibration $Q_1(A_1')$.

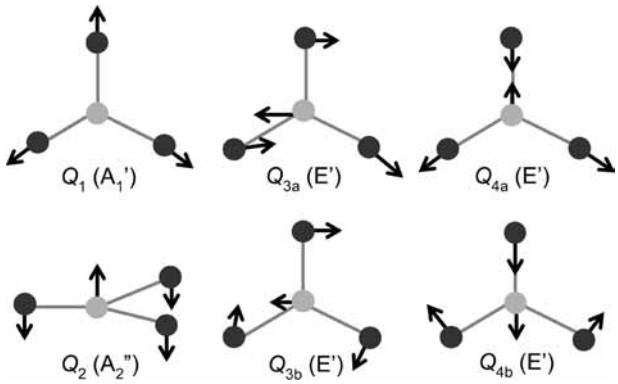

Figure 4. Normal vibrations of the $PrBr_3$ molecule given by the vibrational analysis. $Q_{na}(E')$ and $Q_{nb}(E')$ (n = 3, 4) are doubly degenerate vibrations.

TABLE 4: Oscillator Strengths (LF) ($f \times 10^6$) of $PrBr_3$ in Consideration of Normal Vibrations

modes	$Q_1(A_1')$	$Q_2(A_2'')$	$Q_3(E')^a$	$Q_4(E')^a$
frequencies[b]	196.4	35.4	245.7	45.8
exptl[c]	193	31	236	45
$^3H_6$	0.11[d]	0.10	0.11	0.11
	(−0.18%)[e]	(−6.24%)	(1.11%)	(−0.64%)
$^3F_2$	27.29	26.41	27.29	26.33
	(0.05%)	(−3.15%)	(0.05%)	(−3.47%)
$^3F_3 + {}^3F_4$	4.52	4.49	4.53	4.49
	(−0.01%)	(−0.63%)	(0.11%)	(−0.62%)

[a] The average values of doubly degenerate components in each normal vibration. [b] Frequencies (cm^{-1}) calculated by FDM. [c] Experimental frequencies from ref 48. [d] The upper stand shows oscillator strengths. [e] The lower stand shows relative changes (%).

The oscillator strengths including the vibrationally excited states of each normal vibration and their relative changes from those calculated at the equilibrium structure are shown in Table 4. The relative changes become larger as the frequency of normal vibration becomes smaller, yet they do not exceed about 6%. The out-of-plane bending vibration $Q_2(A_2'')$, the doubly degenerate stretching vibrations $Q_3(E')$, and the doubly degenerate bending vibrations $Q_4(E')$ can lower the molecular symmetry from D_{3h} to C_{3v}, C_s, and C_{2v}, respectively, in which the hypersensitivities can be observed according to Judd[8] as mentioned in the Introduction. Therefore, it is confirmed again that the theory cannot give a consistent explanation for LnX_3 systems. It turns out that the effect of molecular vibration on the f−f intensity is negligibly small and that molecular vibration cannot be a cause of hypersensitivity in contradiction to the previous interpretation by Gruen et al.[7] and Henrie et al.[10]

4.4. Effect of f−d Mixing. We next tried to test the accepted theory by Judd and Ofelt that f−f intensity is induced by the mixing of the opposite parity configuration, such as $4f^{N-1}5d^1$, into the $4f^N$ states. If this interpretation is correct, the oscillator strength should become smaller as the mixing of the 5d component into 4f becomes smaller. We focused attention on only 5d orbitals because the population of 5d orbitals was much larger than that of other virtual orbitals, such as 6s and 6p orbitals. To observe the decrease of the f−d mixing, we shifted 5d orbitals to a higher energy region by adding MCP shift operators of the 5d orbitals to the Hamiltonian. By doing so, the mixing of the 5d components into the 4f orbitals, therefore the mixing of the configurations of $4f^{N-1}5d^1$ to the $4f^N$ states, could be decreased. The oscillator strengths of $PrBr_3$ calculated in this way are shown in Table 5. With the 5d MCP shift operators, the oscillator strengths from $^3H_4$ to ^3P_J (J = 0, 1, 2) were decreased, whereas those of the other transitions were increased contrary to the original expectation. From this result, it is clear that there exist other mechanisms than the f−d mixing for explaining f−f transitions including the hypersensitive transitions.

TABLE 5: Oscillator Strengths (LF) ($f \times 10^6$) of $PrBr_3$ with 5d Shift Operators with Various B_{5d} Values

states	$B_{5d} = 0$	$B_{5d} = 0.1$	$B_{5d} = 0.5$	$B_{5d} = 1.0$	$B_{5d} = 5.0$
$^3H_5$	1.16	1.30	1.88	2.24	2.65
$^3H_6$	0.12	0.11	0.12	0.14	0.18
$^3F_2$	28.08	30.63	43.47	51.79	61.05
$^3F_3$	3.62	3.71	4.86	5.61	5.82
$^3F_4$	1.18	1.23	1.65	1.99	2.98
$^1G_4$	0.12	0.11	0.11	0.12	0.15
$^1D_2$	0.47	0.54	0.77	0.93	1.17
$^1I_6$	3.21	3.18	4.16	4.75	5.27
$^3P_0$	1.68	0.90	0.33	0.55	1.16
$^3P_1$	1.54	0.93	0.56	0.78	1.27
$^3P_2$	0.70	0.53	0.36	0.30	0.24

4.5. Cause of Large Oscillator Strengths of Hypersensitive Transitions. We next examined the oscillator strengths in detail to find out electronic excitations which make dominant contributions to the oscillator strengths. The transition dipole moment is expressed with MO-basis transition density matrix as

$$\mathbf{M}_{FI} = \sum_{f,i} \langle \phi_f | \mathbf{r} | \phi_i \rangle \rho^{FI}(f,i) \equiv \sum_{f,i} \mathbf{m}'(f,i) \qquad (19)$$

Because MOs contain the components of both lanthanide and halogen, we transform MOs to atomic orbitals (AOs) to clarify which excitations, such as those from lanthanide to lanthanide or from ligands to lanthanide, contribute to the oscillator strengths. MOs are expressed in the linear combination of AOs as

$$\phi_i = \sum_s c_{si} \varphi_s^{AO}, \ \phi_f = \sum_r c_{rf} \varphi_r^{AO} \qquad (20)$$

where φ^{AO} is AO and c is the expansion coefficient. Then, eq 19 can be written as

$$\mathbf{M}_{FI} = \sum_{r,s} \langle \varphi_r^{AO} | \mathbf{r} | \varphi_s^{AO} \rangle \sum_{f,i} c_{rf} c_{si} \rho^{FI}(f,i) = \sum_{r,s} \langle \varphi_r^{AO} | \mathbf{r} | \varphi_s^{AO} \rangle P^{FI}(r,s) \equiv \sum_{r,s} \mathbf{m}''(r,s) \qquad (21)$$

where $P^{FI}(r,s)$ is the AO-basis transition density matrix. Here, the oscillator strength from initial states $^{2S+1}L_J$ to final states $^{2S'+1}L'_{J'}$ is written as the summation of the squares of the transition dipole moments over all the states correlated with the initial and final states. Equation 21 can be rewritten by squaring both sides as

$$M_{FI}^2 = \mathbf{M}_{FI} \cdot \sum_{r,s} \mathbf{m}''(r,s) \qquad (22)$$

and then the formula of the oscillator strengths is expressed as follows

$$f(^{2S'+1}L'_{J'} \leftarrow {}^{2S+1}L_J) = A\sum_{F,I}\omega_{FI}M_{FI}^2 = A\sum_{F,I}\sum_{r,s}\omega_{FI}\{\mathbf{m}''(r,s)\cdot\mathbf{M}_{FI}\} \equiv \sum_{r,s}\mu''(r,s) \quad (23)$$

where ω_{FI} is the excitation energy from a state I to a state F and A is $2/3(2J+1)^{-1}$. The values of $\mu''(r,s)$ and the relative intensities defined as

$$\frac{\mu''(r,s)}{f(^{2S'+1}L'_{J'} \leftarrow {}^{2S+1}L_J)} \quad (24)$$

were calculated for $PrBr_3$ and $TmBr_3$ and are shown in Figure 5. Here, the oscillator strengths were classified into four groups, such as μ''(Ln,Ln), μ''(X_3,Ln), μ''(Ln,X_3), and μ''(X_3,X_3), where Ln denotes all the AOs on lanthanide and X_3 denotes all the AOs on halogens. As shown in Figure 5(a-2), in the case of $PrBr_3$, the contributions of μ''(Ln,Ln) dominate the intensities

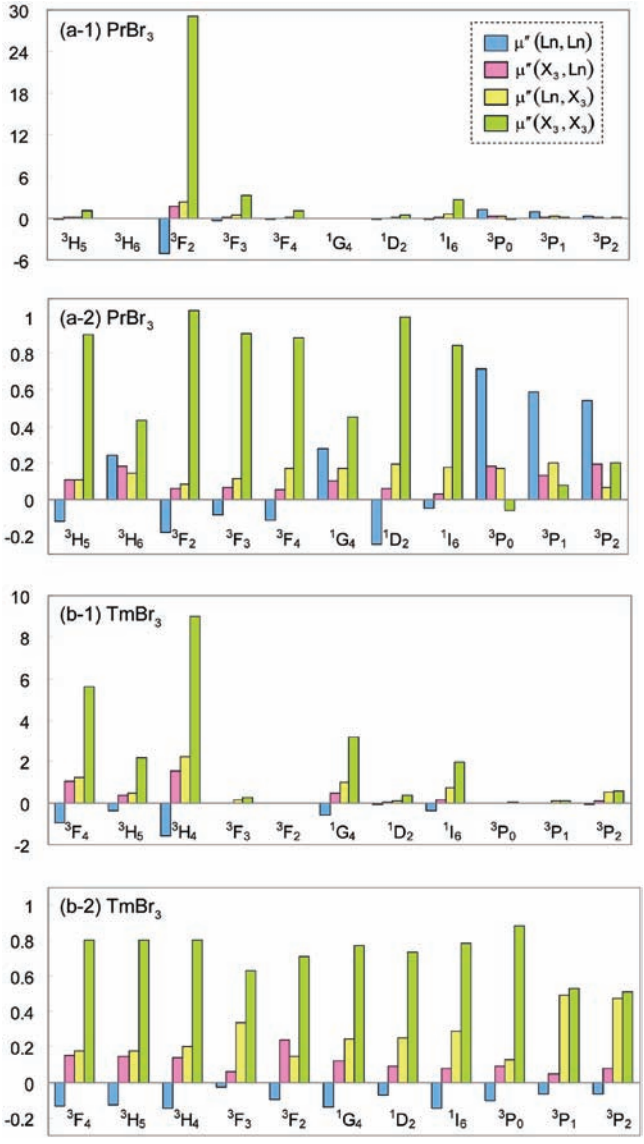

Figure 5. Calculation results of the values of $\mu''(r,s)$ in eq 23 and the relative magnitudes in eq 24. (a-1) and (a-2) are those for each transition from $^3H_4$ of $PrBr_3$. (b-1) and (b-2) are those for each transition from $^3H_6$ of $TmBr_3$. Blue, pink, yellow, and green bars are those for μ''(Ln,Ln), μ''(X_3,Ln), μ''(Ln,X_3), and μ''(X_3,X_3), respectively.

of transitions from $^3H_4$ to ^3P_J ($J = 0, 1, 2$) whereas those of μ''(X_3,X_3) dominate the intensities of other transitions including the hypersensitive transition from $^3H_4$ to $^3F_2$. In the case of $TmBr_3$, as shown in Figure 5(b-2), those of μ''(X_3,X_3) dominate the intensities for almost all transitions including the hypersensitive ones from $^3H_6$ to $^3H_4$ and to $^3F_4$. Recalling the observation in the previous section 4.4, for the transitions from $^3H_4$ to ^3P_J ($J = 0, 1, 2$) of $PrBr_3$, the oscillator strengths became smaller as the f−d mixing became smaller. This observation is consistent with the dominant contributions of μ''(Ln,Ln) because these oscillator strengths are mainly described by the f−d mixing mechanism; that is, excitations between lanthanide atomic orbitals, especially from 4f to 5d, are important. However, there were other transitions whose oscillator strengths were increased with 5d shift operators. The formal charge in LnX_3 is described as $Ln^{3+}(X^-)_3$ and the Ln 5d orbitals are empty. In reality, however, there is a non-negligible amount of charge transfer from ligand halogen atoms to the 5d orbitals (LMCT). When 5d orbitals of lanthanide are shifted to a higher-energy region, the LMCT would be less efficient, and the population in valence p orbitals of halogens is increased. If this is the case, the increase of the contributions of intraligand excitations is expected. As explained in what follows, these intraligand excitations dominate intensities of most of the f−f transitions, therefore the 5d shift operation would increase the oscillator strengths for these transitions. Moreover, for the transitions from $^3H_4$ to $^3H_6$ and to $^1G_4$ of $PrBr_3$ shown in Table 5, while the energy shift B_{5d} was small, the oscillator strengths were decreased with B_{5d} values; however they were increased with larger B_{5d} values. This observation is consistent with the competing contributions of μ''(X_3,X_3) and other $\mu''(r,s)$'s, which are apparent in Figure 5(a-2).

Next, we examined which CSFs affect the values of μ''(X_3,X_3) most significantly. Because the present calculations include only single excitations from the reference CSFs, the pairs of CSFs which contribute to μ''(X_3,X_3) are restricted to the following five types

$$(4f^N \otimes \phi_{X_3} \rightarrow \phi_{Ln^*},\ 4f^N \otimes \phi_{X'_3} \rightarrow \phi_{Ln^*}) \quad (25a)$$

$$(4f^N \otimes \phi_{X_3} \rightarrow \phi_{X_3^*},\ 4f^N \otimes \phi_{X'_3} \rightarrow \phi_{X_3^*}) \quad (25b)$$

$$(4f^N \otimes \phi_{Ln} \rightarrow \phi_{X_3^*},\ 4f^N \otimes \phi_{Ln} \rightarrow \phi_{X'_3{}^*}) \quad (25c)$$

$$(4f^N \otimes \phi_{X_3} \rightarrow \phi_{X_3^*},\ 4f^N \otimes \phi_{X_3} \rightarrow \phi_{X'_3{}^*}) \quad (25d)$$

$$(4f^N,\ 4f^N \otimes \phi_{X_3} \rightarrow \phi_{X'_3{}^*}) \text{ and } (4f^N \otimes \phi_{X_3} \rightarrow \phi_{X'_3{}^*},\ 4f^N) \quad (25e)$$

where ϕ_{X_3} and $\phi_{X_3^*}$ are occupied and virtual MOs of ligands, respectively; ϕ_{Ln} and ϕ_{Ln^*} are occupied and virtual MOs of lanthanide, respectively; $4f^N$ denotes the reference CSFs; and $4f^N \otimes \phi_A \rightarrow \phi_{B^*}$ denotes the CSF that is obtained by one-electron excitation from an occupied MO ϕ_A to a virtual MO ϕ_{B^*}. These pairs of CSFs are classified into three types of $\rho^{FI}(f,i)$ or $\mathbf{m}'(f,i)$, such as $(f,i) = (X_3,X'_3)$, (X_3,X'^*_3), and (X^*_3,X'^*_3), where $(f,i) = (X_3,X'^*_3)$ denotes both (X_3,X'^*_3) and (X'^*_3,X_3) terms. The pairs of CSFs of eqs 25a and 25b contribute to $\mathbf{m}'(X_3,X'_3)$, those of eqs 25c and 25d to $\mathbf{m}'(X^*_3,X'^*_3)$, and those of eq 25e to $\mathbf{m}'(X_3,X'^*_3)$, respectively. To compare these contributions, $\mathbf{m}'(f,i)$

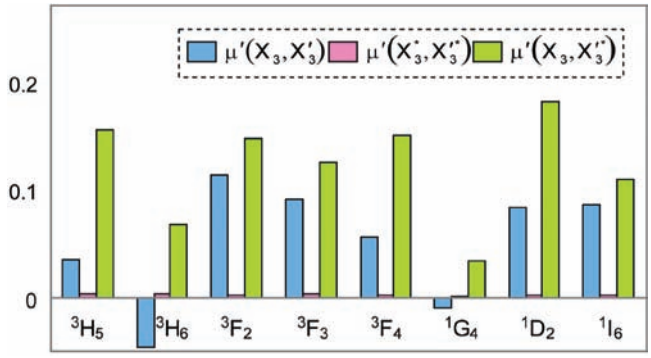

Figure 6. Calculation results of the relative magnitudes of $\mu'(f,i)$ in eq 27 for $PrBr_3$. Blue, pink, and green bars are those for $\mu'(X_3,X'_3)$, $\mu'(X^*_3,X'^*_3)$, and $\mu'(X_3,X'^*_3)$, respectively.

in eq 19 is treated in the same way as eqs 21−23, and then oscillator strengths are written as

$$f(^{2S'+1}L'_{J'} \leftarrow {}^{2S+1}L_J) = A\sum_{F,I}\sum_{f,i}\omega_{FI}\{\mathbf{m}'(f,i)\cdot\mathbf{M}_{FI}\} \equiv \sum_{f,i}\mu'(f,i) \quad (26)$$

The relative magnitude of $\mu'(f,i)$ with respect to the oscillator strength defined as

$$\frac{\mu'(f,i)}{f(^{2S'+1}L'_{J'} \leftarrow {}^{2S+1}L_J)} \quad (27)$$

was calculated for $PrBr_3$ and shown in Figure 6. As is evident here, for many states, the contributions of $\mu'(X_3,X'^*_3)$ and $\mu'(X_3,X'_3)$ are similar in magnitude, whereas those of $\mu'(X^*_3,X'^*_3)$ are very small. Note that the sum of these three types of $\mu'(f,i)$ for each transition in Figure 6 is smaller than the value for the corresponding $\mu''(X_3,X_3)$ in Figure 5(a-2) because the contributions of delocalized virtual MOs between lanthanide and ligands were not accounted for.

In the present first-order CI scheme, an initial state and a final state can be expanded as follows

$$|\Psi_I\rangle = \sum_l b_l|(Ln^N)_l\rangle + \sum_n c_n|(4f^N \otimes \phi_{X_3} \rightarrow \phi_{Ln^*})_n\rangle + \sum_m d_m|(4f^N \otimes \phi'_{X_3} \rightarrow \phi_{X_3^*})_m\rangle + \cdots \quad (28)$$

$$|\Psi_F\rangle = \sum_{l'} b_{l'}|(Ln^N)_{l'}\rangle + \sum_{n'} c_{n'}|(4f^N \otimes \phi_{X'_3} \rightarrow \phi_{Ln^*})_{n'}\rangle + \sum_{m'} d_{m'}|(4f^N \otimes \phi'_{X_3} \rightarrow \phi_{X_3^*})_{m'}\rangle + \cdots \quad (29)$$

where b_l, c_n, and d_m are CI coefficients for intrametal excitation CSFs including $4f^N$ and f−d mixing, LMCT CSFs, and intraligand excitation CSFs, respectively, for the initial state, whereas $b_{l'}$, $c_{n'}$, and $d_{m'}$ are those for the final state. These LMCT and intraligand excitation CSFs represent, respectively, the contributions described by the covalency model[10,11] and the DC model[13−15] mentioned in the Introduction. For most lower lying $4f^N$ states, the magnitudes of the CI coefficients were found to be typically in the following order

$$|b_l|, |b_{l'}| \gg |c_n|, |c_{n'}| > |d_m|, |d_{m'}| \quad (30)$$

that is, the magnitudes of CI coefficients for LMCT CSFs were typically larger than those of intraligand excitation CSFs.

Most of the results in Figure 6 are understandable from the magnitude relation in eq 30. For example, a pair of CSFs in eq 25a, both of which represent LMCT, has a contribution of the order of $c_nc_{n'}$ to the transition density matrix, and that in eq 25e, which represent $4f^N$ and intraligand excitation CSF, has a contribution of the order of $b_ld_{m'}$. From eq 30, these values can be similar in magnitude and result in the competing magnitude of $\mu'(X_3,X'_3)$ and $\mu'(X_3,X'^*_3)$ for most transitions in Figure 6. In a similar manner, a pair of CSFs of eq 25b or eq 25d, both representing intraligand excitations, has a small contribution of the order of $d_md_{m'}$, therefore their contributions to $\mu'(X_3,X'_3)$ and $\mu'(X^*_3,X'^*_3)$ are small; in other words, the contributions to $\mu'(X_3,X'_3)$ come mostly from LMCT CSF pairs and not from intraligand excitation CSF pairs. A pair of CSFs in eq 25c represents metal to ligand charge transfer (MLCT) contributions, whose CI coefficients are in general much smaller than those for LMCT, and their possible contributions to $\mu'(X^*_3,X'^*_3)$ are also small.

From eq 30, it may be expected that CSF pairs of $4f^N$ and LMCT have a large contribution to intensity in the forms of $\mu''(X_3,Ln)$ and $\mu''(Ln,X_3)$ in Figure 5. However, as shown in eq 19, transition dipole moments are given by the trace of dipole matrix elements and transition density matrix elements. In the case of $PrBr_3$, the contributions of dipole matrix elements for these CSF pairs are very small because lower virtual Ln MOs and occupied X_3 MOs do not have a significant overlap. By comparing the results in Figure 5 and also those for PrI_3 and TmI_3 (not shown), in general, the contributions of $\mu''(X_3,Ln)$ and $\mu''(Ln,X_3)$ become increased for heavier Ln and for heavier X. These tendencies are expected since the orbital overlap between lower virtual Ln MOs and occupied X_3 MOs will be increased for heavier Ln due to the so-called lanthanide contraction and for heavier X due to the increased size of X_3 MOs.

These contributions of $\mu''(X_3,Ln)$ and $\mu''(Ln,X_3)$ to transition dipole moments were considered by including LMCT in the previously covalency model.[11] It is however important to emphasize that the dominant contributions of LMCT CSFs to transition dipole moments for most transitions, as analyzed in this study, are not in the forms of $\mu''(X_3,Ln)$ and $\mu''(Ln,X_3)$ but in the form of $\mu''(X_3,X_3)$. Therefore, the dominant contributions represented in eq 25a suggest a different mechanism from those with the covalency model. This difference comes from the difference in magnitudes of the dipole matrix elements; that is, those between occupied X_3 MOs are in general larger than those between lower virtual Ln MOs and occupied X_3 MOs.

From the above consideration, it is understandable that the oscillator strengths of most f−f transitions including hypersensitive transitions in Figure 6 arise from the LMCT and intraligand excitations through their configuration mixings with the dominant configurations of $4f^N$. It is therefore interpreted that the reason of hypersensitive transitions in LnX_3 molecules is the significant contribution of these effects which do not work much in aqueous Ln^{3+} systems. It is also interpreted that the oscillator strengths of hypersensitive transitions are sensitive to the surrounding environment as a direct reflection of the sensitivity of these mixed states to small changes of ligands.

Recalling the observation in previous section 4.2, the components of large f−f transition dipole moments were in the direction of the molecular plane ($x,y \in E'$). Therefore the

irreducible representation of the $X_3 \rightarrow X_3^*$ portion must be E′ for the transition dipole moment between the pairs of CSFs (25e) to have a large value. This symmetry requirement limits both ϕ_{X_3} and $\phi_{X_3^*}$ to have σ symmetry or π symmetry. Our separate calculations on an artificial molecule of $(X^-)_3$, whose structure was taken from LnX_3, showed that it had large transition dipole moments of e′ symmetry for some one-electron excitations from valence σ symmetry MOs (e′) to lower unoccupied σ symmetry MOs (a_1',e′) while those in the z direction were much smaller. These results are consistent with the fact that the f−f transition dipole moments had large values only in the direction of the molecular plane.

Next, we compared our results with the DC model, which considers the effect of intraligand polarized type excitation. In the DC model, the dipole strength is derived in the same way as the Judd−Ofelt theory by adding intraligand excitation configurations to the opposite parity configurations as follows

$$|\Psi_{4f^N}\rangle = |(4f^N)_a\rangle + \sum_{b,l} \frac{\langle (Ln^N)_b \otimes (\phi_{X_3} \rightarrow \phi_{X_3^*})_l | V | (4f^N)_a \rangle}{E_a - E_b - E_l} |(Ln^N)_b \otimes (\phi_{X_3} \rightarrow \phi_{X_3^*})_l\rangle \quad (31)$$

where V denotes the intersystem Coulombic potential whose perturbation matrix element can be approximately expanded in the product of f−f transition quadrupole moment of lanthanide and transition dipole moment of ligand.[13] Comparing eq 31 and eq 28, it is obvious that the essential part of the DC model, that is, the Coulombic correlation between the transition quadrupole moment of Ln and the transition dipole moment of the X_3 portion, can be accounted for in the present first-order CI scheme. In the DC model, the expression of f−f transition dipole moments yields the squares of transition dipole moments of the ligand, which can be further reduced to the components of the polarizability tensor of the ligand.[13] Therefore, including the intraligand excitation contributions in the present first-order CI scheme corresponds to considering the effect of the dynamic coupling between Ln and the X_3 portion, with ligand polarization taken into account.

As Tables 2 and 3 show, the oscillator strengths of hypersensitive transitions are larger than those of others. Moreover, as Figure 5 shows, these hypersensitive transitions are dominated by $\mu''(X_3,X_3)$, and this dominance of $\mu''(X_3,X_3)$ can also be seen in most other transitions. This observation is consistent with the DC model. In this model, only the expression of the Ω_t parameter is different from those of the original Judd−Ofelt theory. The Ω_t parameters of the DC model contain the polarizability of the ligand, and the ligand-polarization contributions to these parameters are very large only for the Ω_2 (i.e., $\Delta J \leq 2$). Therefore, it is interpreted that the magnitude relation between transitions is caused by the magnitude relation of the matrix element of reduced tensor operator $U^{(2)}$,[50] because Ω_4 and Ω_6 are very small. In other words, the mechanism of the DC model can be adapted to not only so-called hypersensitive transitions but also other transitions with $\Delta J \leq 2$. In this way, the semiempirical DC model could explain the hypersensitivity of transitions with $\Delta J \leq 2$. However, we emphasize that our ab initio calculations showed that the transitions with very large contributions of $\mu''(X_3,X_3)$ are not limited to the case of $\Delta J \leq 2$. It is suggested that the neglect of the LMCT contributions in the DC model may be a cause of these differences.

As Tables 2 and 3 show, the oscillator strengths of LnI_3 are larger than those of $LnBr_3$. To explain the difference between ligands, we tested the effect of magnitude of the SO effect by changing the values of Z_{eff} and proved that the SO effect of X_3 on the oscillator strength was very small. Therefore, considering the DC model containing the polarizability of ligand in Ω_t and the results of these test calculations, it is interpreted that the magnitude order between ligands seen in Tables 2 and 3 is explained by that of polarizability of ligands. In summary, to contain all the effects in the evaluations of oscillator strengths, ab initio calculations should be carried out.

5. Conclusions

In this work, we have studied the oscillator strengths of f−f transitions including hypersensitive transitions of LnX_3 (Ln = Pr, Tm; X = Br, I) based on the multireference spin−orbit configuration interaction (SOCI) method. To examine the accuracy of calculation, the oscillator strengths in LF, VF, and VF with SO correction terms were compared, and the additional SO correction terms for VF were found to be of little importance. We compared several calculation methods and employed the model core potential (MCP) method[31,36] to treat only valence electrons with keeping the nodal feature in valence orbitals. We coded and attached a program to compute transition density matrix with graphical unitary group approach (GUGA) both in LF and VF. With these methods, we could calculate the oscillator strengths of LnX_3 quantitatively with LF. It was found that quantitative molecular calculations with VF are more difficult than those with LF.

We examined the cause of hypersensitivity by focusing attention on the effect of molecular vibration, f−d mixing, ligand to metal charge transfer (LMCT), and ligand polarization. It is concluded that the effect of the molecular vibration on the oscillator strengths is very small and that the oscillator strengths of most f−f transitions including hypersensitive transitions arise from both the LMCT and dynamic-coupled intraligand excitations through their configuration mixings with the dominant configurations of $4f^N$.

It is true that the semiempirical DC model[13−15] containing the effect of ligand-polarization contributions could explain the hypersensitivity and the magnitude relation of oscillator strengths between transitions and between ligands for transitions with $\Delta J \leq 2$, but there are other transitions for which the DC model could not explain these properties. In summary, it is only ab initio methods that could contain all the important effects, such as ligand polarization, LMCT, and SO interaction.

Acknowledgment. This work was supported in part by Grants-in-Aids for Scientific Research from MEXT, Japan. A part of the computations was carried out using the computer facilities at the Research Center for Computational Science, Okazaki National Institutes. The authors acknowledge Mr. E. Sanoyama and Dr. M. Morita for their unpublished preliminary works and Mr. K. Saito in Kyoto University for the discussion on the effect of molecular vibration on oscillator strength.

References and Notes

(1) Judd, B. R. *Phys. Rev.* **1962**, *127*, 750.
(2) Ofelt, G. S. *J. Chem. Phys.* **1962**, *37*, 511.
(3) Görller-Varland, C.; Binnemans, K. Spectral intensities of f-f transitions. In *Handbook on the Physics and Chemistry of Rare-Earths*; Gschneider, K. A., Eyring, L., Eds.; Elsevier: Amsterdam, 1998; Vol. 25, pp 101−264.
(4) Jørgensen, C. K.; Judd, B. R. *Mol. Phys.* **1964**, *8*, 281.
(5) Peacock, R. D. *Struct. Bonding (Berlin)* **1975**, *22*, 83.
(6) Gruen, D. M.; DeKock, C. W. *J. Chem. Phys.* **1966**, *45*, 455.
(7) Gruen, D. M.; DeKock, C. W.; McBeth, R. L. *Adv. Chem. Ser.* **1967**, *71*, 102.

(8) Judd, B. R. *J. Chem. Phys.* **1966**, *44*, 839.
(9) Nieuwport, W. C.; Blasse, G. *Solid State Commun.* **1966**, *4*, 227.
(10) Henrie, D. E.; Choppin, G. R. *J. Chem. Phys.* **1968**, *49*, 477.
(11) Henrie, D. E. *Coord. Chem. Rev.* **1976**, *18*, 199.
(12) Peacock, R. D. *Mol. Phys.* **1977**, *33*, 1239.
(13) Mason, S. F.; Peacock, R. D.; Stewart, B. *Mol. Phys.* **1975**, *30*, 1829.
(14) Mason, S. F.; Peacock, R. D.; Stewart, B. *Chem. Phys. Lett.* **1974**, *29*, 149.
(15) Peacock, R. D. *J. Mol. Struct.* **1978**, *46*, 203.
(16) Newman, D. J.; Balasubramanian, G. *J. Phys. C* **1975**, *8*, 37.
(17) Reid, M. F.; Richardson, F. S. *Chem. Phys. Lett.* **1983**, *95*, 501.
(18) Reid, M. F.; Richardson, F. S. *J. Chem. Phys.* **1983**, *79*, 5735.
(19) Reid, M. F.; Richardson, F. S. *J. Chem. Phys.* **1984**, *88*, 3579.
(20) Matsika, S.; Pitzer, R. M.; Reed, D. T. *J. Phys. Chem. A* **2000**, *104*, 11983.
(21) Hafner, P.; Schwarz, W. H. E. *J. Phys. B* **1978**, *11*, 2975.
(22) Wadt, W. R. *Chem. Phys. Lett.* **1982**, *89*, 245.
(23) Pitzer, R. M.; Winter, N. W. *J. Phys. Chem.* **1988**, *92*, 3061.
(24) Pitzer, R. M.; Winter, N. W. *Int. J. Quantum Chem.* **1991**, *40*, 773.
(25) Ermler, W. C.; Lee, Y. S.; Christiansen, P. A.; Pitzer, K. S. *Chem. Phys. Lett.* **1981**, *81*, 70.
(26) Shepard, R.; Shavitt, I.; Pitzer, R. M.; Comeau, D. C.; Pepper, M.; Lischka, H.; Szalay, P. G.; Ahlrichs, R.; Brown, F. B.; Zhao, J.-G. *Int. J. Quantum Chem. Symp.* **1988**, *22*, 149.
(27) Saito, K.; Eishiro, Y.; Nakao, Y.; Sato, H.; Sakaki, S. Annual Meeting of Japan Society for Molecular Science 2008, 1E18 (in Japanese).
(28) Yabushita, S.; Zhang, Z.; Pitzer, R. M. *J. Phys. Chem. A* **1999**, *103*, 5791.
(29) Cundari, T. R.; Stevens, W. J. *J. Chem. Phys.* **1993**, *98*, 5555.
(30) Dolg, M.; Stoll, H.; Preuss, H. *J. Chem. Phys.* **1989**, *90*, 1730.
(31) Sakai, Y.; Miyoshi, E.; Tatewaki, H. *J. Mol. Struct.: THEOCHEM* **1998**, *451*, 143.
(32) MCP online library: http://meg.cube.kyushu-u.ac.jp/∼meg/MCP1.html.
(33) van Piggelen, H. U.; Nieuwpoort, W. C.; van der Velde, G. A. *J. Chem. Phys.* **1980**, *72*, 3727.
(34) Martin, W. C.; Zalubas, R.; Hagan, L. *Atomic Energy Levels - The Rare-Earth Elements: The Spectra of Lanthanum, Cerium, Praseodymium, Neodymium, Promethium, Samarium, Europium, Gadolinium, Terbium, Dysprosium, Holmium, Erbium, Thulium, Ytterbium, and Lutetium*; National Bureau of Standards: Washington D. C., 1978.
(35) Hargittai, M. *Coord. Chem. Rev.* **1988**, *91*, 35.
(36) Miyoshi, E.; Sakai, Y.; Tanaka, K.; Masamura, M. *J. Mol. Struct.: THEOCHEM* **1998**, *451*, 73.
(37) Moore, C. E. *Atomic energy levels as derived from the analysis of optical spectra*; National Bureau of Standards: Washington D. C., 1971; Vols. 2−3.
(38) Shavitt, I. The graphical unitary group approach and its application to direct configuration-interaction calculations. In *The Unitary Group for the Evaluation of Electronic Energy Matrix Elements*; Hinze, J., Ed.; Lecture Notes in Chemistry 22; Springer: Berlin, 1981; pp 51−99.
(39) Shavitt, I. Unitary group approach to configuration interaction calculations of the electronic structure of atoms and molecules. In *Mathematical Frontiers in Computational Chemical Physics*; Truhlar, D. G., Ed.; Springer: Berlin, 1988; pp 300−349.
(40) Schmidt, M. W.; Baldridge, K. K.; Boatz, J. A.; Elbert, S. T.; Gordon, M. S.; Jensen, J. H.; Koseki, S.; Matsunaga, N.; Nguyen, K. A.; Su, S.; Windus, T. L.; Dupuis, M.; Montgomery, J. A., Jr. *J. Comput. Chem.* **1993**, *14*, 1347.
(41) McCullough, E. A., Jr.; Wyatt, R. E. *J. Chem. Phys.* **1971**, *54*, 3578.
(42) Cerjan, C.; Kulander, K. C. *Comput. Phys. Commun.* **1991**, *63*, 529.
(43) Sugawara, M.; Kato, M.; Fujimura, Y. *Chem. Phys. Lett.* **1991**, *184*, 203.
(44) Pacios, L. F.; Christiansen, P. A. *J. Chem. Phys.* **1985**, *82*, 2664.
(45) Yu, J.; Baker, J. D.; Zerner, M. C. *Int. J. Quantum Chem. Symp.* **1992**, *26*, 475.
(46) Sanoyama, E.; Kobayashi, H.; Yabushita, S. *J. Mol. Struct.: THEOCHEM* **1998**, *451*, 189.
(47) Cundari, R. T.; Sommerer, S. O.; Strohecer, L. A.; Tippett, L. *J. Chem. Phys.* **1995**, *102*, 7058.
(48) Tsukamoto, S.; Mori, H.; Tatewaki, H.; Miyoshi, E. *Chem. Phys. Lett.* **2009**, *474*, 28.
(49) Girichev, N. I.; Girichev, G. V.; Shlykov, S. A.; Krasnov, A. V.; Zakharov, A. V.; Krasnova, O. G. *J. Struct. Chem.* **2004**, *45*, 47.
(50) Carnall, W. T.; Firlds, P. R.; Wybourne, B. G. *J. Chem. Phys.* **1965**, *42*, 3797.

JP9049507